The conformations of narasin–metal complexes in solution determined by NMR spectroscopy

Tamas Martinek,[a] Frank G. Riddell*[b] and Craig F. Wilson[b]

[a] *Institute of Pharmaceutical Chemistry, Albert Szent Gyorgyi Medical University, Szeged, Hungary*
[b] *School of Chemistry, The University of St Andrews, St Andrews, UK KY16 9LT*

Received (in Cambridge, UK) 12th July 2000, Accepted 14th August 2000
First published as an Advance Article on the web 22nd September 2000

The structures in solution of the Na^+, K^+, Rb^+ and Cs^+ salts of narasin have been determined by the use of NOESY distance restraints and molecular modelling. As the size of the metal ion increases the same set of six oxygen atoms remain co-ordinated to the metal but the metal to oxygen distances increase according to the known atomic radii of the ions. Increasing ion size is accommodated by the molecule in two principal ways. As the size of the metal ion increases there is an increase in the H–C(12)–C(13)–H dihedral angle. There is a "head to tail" hydrogen bond (OH(11)$\cdots$O(1)) in the Na^+, K^+ and Rb^+ salts which is much weaker in the Cs^+ salt. There is a relatively strong hydrogen bond between OH(4) and O(2) in all four salts and a much weaker hydrogen bond between OH(8) and O(2) seen only in the Na^+ salt. The relative tightness of the binding increases as the metal ion size increases.

Introduction

The ionophoric antibiotics have been studied in great detail and still continue to attract considerable interest. They have biological activity because of their ability to mediate membrane transport of the alkali metal ions.[1] Their ability to form lipid soluble cation complexes which act as ion carriers has led to their use in biology and biophysics. One of the most intriguing aspects of these compounds is the extreme variability in complexation affinities which they can display within a given cation series.[2]

Narasin (4-methylsalinomycin)[3,4] (**1**), an ionophoric compound isolated from *Streptomyces aurofaciens*, with a preference for complexing sodium, is used commercially as a coccidiostat in conjunction with other antimicrobial agents (as Monteban and Maxiban) and has been studied previously by ^{1}H NMR,[5,6] molecular model building[7] and transport studies.[8–10]

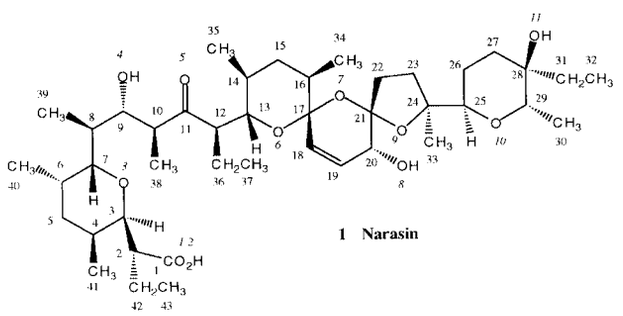

1 Narasin

There are two main items of chemical interest concerning the ionophoric antibiotics. The first is their membrane behaviour: the kinetics and mechanism of the transport process and the membrane stability of the complex. The second is the molecular structure of the complex and the way that it influences the kinetics, mechanism and stability in the membrane. Ion transport by narasin has been extensively studied;[8–10] however, little detailed structural information about its complexes is available. In particular there is no published structural study by X-ray diffraction.

The NMR studies mentioned above combined with molecular model building have suggested that in low polarity environments the molecule assumes a pseudocyclic conformation, most likely stabilised by intramolecular hydrogen bonds.[5] Here the cation-ligating oxygens are directed towards the interior of the molecule whilst the hydrophobic alkyl residues are pointed outwards. This conformation, in a biological membrane, would facilitate dissolution in the hydrophobic interior of the lipid bilayer. It should, however, be remembered that the cation complexation step, which initiates the transport reaction, occurs in a more polar environment where the factors influencing ionophore conformation are significantly different.

Suggestions have been made previously and verified that in narasin that the bonds between C(10) and C(13), and between C(24) and C(25) are "hinge regions" where the greatest molecular flexibility can occur.[5,10] Further studies on the dihedral angles of these hinge areas in the molecule arrived at the conclusion that narasin is as effective a protonophore as it is a K^+ and Na^+ ionophore.[11]

Kinetic measurements of alkali metal ion transport in erythrocytes suggest preferential transport of K^+ over Na^+,[12] and equilibrium selectivity for uptake of Na^+ and K^+ ions in DPMC vesicles agrees with this.[13] This is somewhat different in studies of respiring mitochondria, which suggest the opposite selectivity. Riddell and Tompsett studied alkali metal ion transport in phosphatidylcholine vesicles.[10] They observed that potassium was transported more rapidly than sodium but that sodium formed the marginally more stable complex.

No structural study has been reported on narasin either by X-ray diffraction or by 2D NMR methods. However, the very closely related compound salinomycin (lacks the methyl at position 4 in narasin) has been studied by both methods. Sodium salinomycin, recrystallised from water–acetonitrile, has been studied by X-ray diffraction.[14] Two independent molecules were observed in the crystalline asymmetric unit with different coordination patterns to the sodium. Water molecules were observed as part of the coordination spheres of the penta- and the hexa-coordinate sodium ions. In the case of the hexa-coordinate sodium one of the two waters may have arisen from disorder in the coordination pattern for the molecule and represent sodium in a partially filled coordination site. In terms

 DOI: 10.1039/b005618i

Table 1 Ionic radii of the alkali metals (pm)[a]

Metal	*r*/pm	% increase relative to previous entry
Lithium	76	
Sodium	102	34
Potassium	138	35
Rubidium	152	10
Caesium	167	10

[a] Taken from reference 18 (refers to octahedral co-ordination).

of our (narasin) numbering system the four salinomycin oxygen atoms to coordinate to sodium are oxygens *2*, *5*, *8* and *10*. In contrast to the structure of sodium monensin one of the oxygens from the carboxylate group was observed to coordinate to the sodium ion.

NMR methods have been used twice to obtain the solution structure of sodium salinomycin.[14,15] The work of Paulus *et al*.[14] shows differences in the conformation of the complex in a polar solvent (DMSO) and a lower polarity solvent ($CDCl_3$). The coordination pattern they obtained for the sodium ion was to (in our nomenclature) oxygens *1*, *2*, *5*, *8* and *10*. The earlier study by Mronga *et al*.[15] suggested a penta-coordinate sodium in which oxygens *2*, *4*, *5*, *9* and *10* participate. They identified hydrogen bonds from O(8)H to O(2) and to O(4).

Both the X-ray and the NMR studies on sodium salinomycin mentioned above identified a hydrogen bond tying down the head of the molecule between O(4) and the carboxylate group and a head to tail hydrogen bond from O(11) to the carboxylate group tying the head and tail of the molecule together.

There are two advantages of the NMR method as used in the studies above and by ourselves to study sodium tetronasin[16] and sodium, potassium and rubidium monensin.[17] These are its ability to simulate molecular dynamic processes and, being different from solid state methods, it deals with isolated molecules in solution. Despite these advantages there is one crucial disadvantage. This is that it depends on molecular modeling, which in turn is critically dependent upon the type of force field employed. Solution NMR (especially 2D–3D NMR) and transport studies using NMR can assist in the understanding of the mechanisms by which the hydrated metal ions are taken into the complex and the way in which the complex releases the metal ion back into the aqueous solution.

Table 1 shows the ionic radii of the alkali metals. This table also shows the % change in ionic radius on descending the group. Thus, the changes in size from Li^+ to Na^+ and from Na^+ to K^+ are much more important than the changes from K^+ to Rb^+ and Rb^+ to Cs^+. There has been much discussion in the literature about the "hinge regions" in salinomycin and narasin. A coherent study of the narasin complexes as the radius of the metal ion is increased from Li^+ to Cs^+ should provide clear evidence of the regions of the molecule in which there is sufficient flexibility to facilitate the folding and unfolding processes, and which of the hinge bonds is the most flexible.

Results and discussion

The NMR samples were prepared by vigorously stirring a $CDCl_3$ solution of narasin acid with a saturated aqueous solution of the metal carbonate. The carbonates were chosen because of their basic nature and because their high solubility in water should boost a mass action effect to insert the metal. The $CDCl_3$ layer was then separated and filtered into the NMR tube through a short column of the anhydrous metal carbonate. There was only evidence of one principal species in the ^1H spectra every case confirming that the 1 : 1 M^+–narasin complex is the almost exclusive product.

The assignment of the ^1H NMR spectra of the narasin salts was straightforward. The resonance of H(20) was readily identified in the 1D ^1H spectrum at *ca.* 4.00 ppm. Starting from this resonance the use of COSY connectivities gave the assignments of ring C (ring labelling A–E runs from left to right in structure **1**. H(25) at *ca.* 3.40 ppm was used to assign most of ring D and E again using COSY connectivities. H(13) was then used to to assign ring B and H(12) and the substituent ethyl group C(36) and C(37). H(10) at *ca*. 2.65 ppm could then be used to assign the rest of the molecule. Assignment was made easier by checking against the values given in reference 6 and satisfactory agreement was found in all but a few cases. Chemical shifts are given in Table 2.

Table 2 ^1H chemical shifts (δ_H relative to TMS) of the alkali metal complexes of narasin

	δ_H			
Atom	Na	K	Rb	Cs
2	2.80	2.78	2.79	2.87
3	3.84	3.81	3.82	3.84
4	2.29	2.28	2.28	2.29
5d	1.79	1.82	1.82	1.84
5u	1.40	1.39	1.37	1.37
6	1.83	1.84	1.86	1.89
7	3.74	3.75	3.79	3.91
8	1.45	1.47	1.47	1.51
9	4.24	4.29	4.27	4.17
10	2.67	2.64	2.64	2.66
12	2.69	2.62	2.59	2.59
13	3.53	3.65	3.78	3.94
14	1.73	1.74	1.72	1.68
15d		1.65	1.64	1.64
15u	1.15	1.15	1.14	1.11
16	1.71	1.74	1.75	1.72
18	6.02	6.06	6.07	6.17
19	6.02	6.11	6.13	6.17
20	4.05	3.99	3.99	4.03
22d	2.33	2.42	2.36	2.32
22u	1.87	2.01	2.12	1.96
23d	2.00	1.89	1.90	1.89
23u	1.87	1.89	1.79	1.89
25	3.40	3.45	3.46	3.39
26d	2.11	2.07	2.05	2.00
26u	1.35	1.38	1.41	1.41
27d	1.70	1.69	1.70	1.70
27u	1.47	1.50	1.50	1.53
29	4.31	4.16	4.04	3.92
30	1.26	1.24	1.23	1.21
31	1.29	1.33	1.35	1.34
32	0.90	0.92	0.92	0.91
33	1.79	1.64	1.55	1.58
34	0.71	0.73	0.73	0.72
35	0.89	0.93	0.95	0.95
36d	1.94	1.96	1.94	1.91
36u	1.33	1.35	1.37	1.40
37	0.77	0.77	0.77	0.78
38	0.87	0.84	0.82	0.84
39	0.71	0.71	0.71	0.74
40	0.92	0.92	0.92	0.93
41	0.90	0.90	0.90	0.93
42d	1.67	1.62	1.60	1.53
42u	1.55	1.57	1.56	1.53
43	0.93	0.90	0.89	0.90

The narasin salts in this paper are roughly globular molecules with a relatively low molecular weight (NaNar = 788 amu) and molecular tumbling correlation times in the ns region. Consequently they produce rather low intensity NOESY cross-peaks and so optimisation of the signal to noise ratio (S/N) in the NOESY spectra assumes a special importance. NOESY spectra were obtained with mixing times of between 100 ms and 700 ms. The NOE build up rates proved to be essentially linear in the 0–400 ms range. The longer mixing times produced a levelling off in peak intensity. The NOESY cross peak intensities at 400 ms were then adopted as a compromise between acceptable S/N and linearity for the establishment of distance restraints. ROESY spectra offer an alternative in systems where NOESY

Table 3 Observed distances (Å) from NOESY spectra of M^+ narasin salts, applied restraints and back-calculated distances

Na					K				
Proton pair		Exp. dist./Å	Upper boundary/Å	Back-calc. dist./Å	Proton pair		Exp. dist./Å	Upper boundary/Å	Back-calc. dist./Å
H19	H20	2.5	3.0	2.4	H10	Me38	2.2	2.7	2.6
H18	H13	1.8	2.1	2.0	H10	Me39	2.3	2.8	2.6
H9	H10	2.5	3.0	2.8	H12	H14	2.4	3.0	2.7
H9	H8	2.0	2.5	2.3	H12	Me35	2.3	2.8	2.6
H29	Me30	2.2	2.7	2.6	H12	Me37	2.5	3.1	2.9
H29	Me32	2.6	3.2	2.8	H13	H12	1.9	2.8	2.3
H9	Me38	2.6	3.2	2.9	H13	H10	1.9	2.8	2.3
H3	H2	2.6	3.2	2.8	H13	H14	2.6	3.1	2.8
H7	H2	2.0	2.4	2.3	H13	H15u	2.2	2.7	2.5
H13	H12	1.8	2.7	2.3	H13	Me35	2.6	3.2	2.9
H13	H10	1.8	2.7	2.4	H15d	H15u	2.0	2.4	1.8
H3	H4	1.9	2.3	2.2	H15d	Me34	2.5	3.1	3.0
H7	H6	1.9	2.3	2.3	H16	Me34	2.5	3.0	2.6
H25	Me33	2.4	3.0	2.8	H18	H20	3.2	3.9	3.5
H25	H23u	2.2	2.7	2.5	H18	H13	1.9	2.4	2.0
H25	H26u	2.1	2.6	2.4	H18	H15u	2.2	2.7	2.3
H25	Me30	2.3	2.8	2.7	H18	Me34	3.3	4.0	3.4
H13	H15u	2.1	2.6	2.4	H19	H20	2.5	3.0	2.4
H3	Me41	2.6	3.2	3.0	H19	Me34	3.8	4.6	3.8
H13	Me35	2.6	3.2	3.0	H2	H5d	1.9	2.3	2.3
H7	Me39	2.6	3.2	3.0	H2	Me43	2.5	3.0	2.9
H2	H5d	2.0	2.4	2.3	H20	H22d	2.3	2.8	2.5
H2	Me43	2.3	2.8	2.9	H20	Me34	2.6	3.2	2.7
H12	Me37	2.5	3.1	2.9	H20	H22u	2.4	3.0	2.6
H10	Me39	2.4	2.9	2.7	H22d	H22u	1.6	1.9	1.7
H22d	H23u	1.5	1.9	2.2	H25	H26u	2.1	2.6	2.4
H26d	H26u	1.6	2.0	1.8	H25	Me30	2.4	2.9	2.6
H4	Me41	2.2	2.6	2.6	H25	Me33	2.5	3.1	2.8
H23d	H23u	1.7	2.1	1.8	H26d	H27d	1.9	2.3	2.3
H23d	Me33	2.3	2.9	2.8	H26d	H26u	1.6	2.0	1.8
H6	H5u	1.6	1.9	2.3	H27d	H27u	1.6	2.0	1.8
H36d	H36u	1.7	2.1	1.8	H8	Me40	2.2	2.7	2.6
H6	Me40	2.3	2.8	2.7	H27u	Me32	2.3	2.8	2.7
H6	Me39	2.5	3.1	2.7	H29	Me30	2.3	2.9	2.6
H16	Me34	2.3	2.8	2.6	H29	Me32	2.9	3.5	3.6
H27d	H27u	1.6	2.0	1.8	H3	H2	2.7	3.3	2.8
H8	Me38	2.4	2.9	2.6	H3	H4	1.9	2.4	2.2
H8	Me40	2.4	2.9	2.7	H3	Me41	2.7	3.4	3.1
H8	Me39	2.7	3.2	2.8	H36d	H36u	1.7	2.0	1.8
H18	Me34	3.2	3.9	3.3	H4	H5u	2.2	2.7	2.5
H18	H15u	2.3	2.8	2.5	H4	Me41	2.2	2.7	2.5
H7	H8	2.9	3.5	2.9	H5u	Me41	2.0	2.4	2.8
H13	H14	2.5	3.1	2.8	H6	H5u	1.5	1.9	2.3
H20	Me34	2.7	3.3	3.0	H7	H2	2.7	3.3	2.5
H4	H5u	2.2	2.7	2.5	H7	H6	1.9	2.3	2.3
H26d	H27d	2.4	2.9	2.4	H7	H8	2.6	3.2	2.9
H9	H7	2.5	3.1	2.9	H7	Me39	2.8	3.5	3.0
H9	Me39	3.3	4.0	4.0	H6	Me39	2.3	2.8	2.6
H7	Me40	3.2	3.9	4.1	H8	Me38	2.3	2.8	2.6
H13	Me34	3.5	4.2	4.9	H8	Me39	2.5	3.1	2.7
H20	H22d	2.2	2.7	2.6	H9	H7	2.5	3.0	2.9
H20	H22u	2.4	3.0	2.6	H9	H10	2.6	3.2	2.8
H22d	H26u	2.5	3.0	2.9	H9	H8	2.0	2.5	2.3
H23u	H26u	2.1	2.5	2.3	H9	Me38	2.6	3.2	2.9
H25	H27u	2.3	2.8	2.5	H9	H27u	2.3	2.8	2.6

cross peaks are small but were not used here as adequate S/N was obtainable on a reasonable timescale.

Distances were calculated using the isolated spin pair approximation (ISPA) which applies and serves as a reliable estimation for the restrained molecular dynamics (MD) calculations in this case. The reference distance was taken as 1.78 Å, an approximation for the average intensity of cross peaks of the geminal pairs (H261–H262 and H271–H272) as determined crystallographically. The distance upper and lower boundaries were determined by an experimental error of ±10% of the observed experimental distance from NOESY integrals. A list of the experimental distances, the applied restraints and back-calculated distances in the final model is given in Table 3. Agreement between the observed and calculated distances from the models is particularly good for the majority of the proton pairs except for the restraints in the surrounding area of the spiro-ketal system (ring B, C, and D) where the comparison gave satisfactory results. Back-calculated distances are from averaging over the entire time course of a 100 ps molecular dynamics simulation using the NOESY distance restraints.

Lower and upper bounds of distance restraints were fixed at ±10% of the observed distance from the NOESY spectra. In the case of the Na^+ and K^+ salts a bound of ±20% was applied for the cross peaks for H10–H13 and H12–H13 because of the partial overlap of the signals causing a larger integration error.

The starting model was made using the 'Builder' program from Insight (the molecular modelling program used) which converts a 2D sketch to a 3D model where the absolute

Table 3 (*Continued*)

Rb					Cs				
Proton pair		Exp. dist./Å	Upper boundary/Å	Back-calc. dist./Å	Proton pair		Exp. dist./Å	Upper boundary/Å	Back-calc. dist./Å
H19	H20	2.5	3.1	2.4	H19	H20	2.3	2.8	2.3
H18	H13	2.5	3.0	2.2	H18	H13	1.8	2.2	2.0
H18	H15u	2.1	2.6	2.3	H7	H2	1.9	2.3	2.0
H9	H7	2.6	3.2	3.0	H3	H2	2.6	3.2	2.8
H3	H2	2.1	2.6	2.8	H9	H10	2.6	3.2	2.7
H7	H2	2.0	2.4	2.2	H9	H8	2.5	3.1	2.2
H13	H10	2.1	2.5	2.2	H9	Me40	4.0	4.9	4.6
H9	H10	2.6	3.2	2.8	H9	Me38	2.6	3.2	2.9
H3	H4	1.9	2.3	2.1	H9	Me39	3.5	4.3	3.8
H25	H26d	3.4	4.1	3.2	H20	H22d	2.5	3.1	2.4
H25	H23d	2.3	2.9	2.7	H20	H22u	2.5	3.0	2.5
H7	H6	1.9	2.3	2.3	H20	Me34	3.2	3.9	3.0
H13	H13	2.1	2.6	2.4	H13	H10	2.1	2.5	2.2
H13	H14	2.6	3.2	2.8	H13	H12	2.2	2.7	2.4
H7	H8	2.5	3.1	2.9	H13	H14	2.7	3.3	2.7
H9	H8	2.0	2.4	2.2	H13	H15u	2.2	2.7	2.5
H25	H26u	2.1	2.6	2.5	H13	Me35	2.6	3.1	2.8
H25	Me33	2.5	3.1	2.8	H7	H8	2.7	3.2	2.8
H29	Me30	2.3	2.8	2.6	H7	Me39	3.0	3.7	2.9
H13	H15u	2.3	2.8	2.5	H3	H4	2.1	2.6	2.1
H25	Me30	2.3	2.8	2.6	H3	Me41	2.5	3.1	2.8
H29	Me32	2.7	3.3	2.8	H25	H26d	2.7	3.3	3.1
H3	Me41	2.6	3.2	3.0	H25	Me33	2.6	3.1	2.7
H13	Me35	2.6	3.1	2.9	H25	H26u	2.2	2.7	2.5
H20	Me34	2.4	3.0	2.7	H25	Me30	2.3	2.8	2.6
H7	Me39	2.6	3.2	3.0	H2	H5d	2.0	2.5	2.3
H9	Me38	2.5	3.1	3.0	H2	Me43	2.5	3.0	2.9
H9	Me39	3.3	4.0	3.9	H10	Me35	2.8	3.4	3.0
H2	H5d	2.2	2.6	2.4	H10	Me38	2.4	2.9	2.6
H12	H14	2.2	2.7	2.6	H10	Me39	2.4	2.9	2.6
H4	H5u	2.1	2.5	2.4	H12	H14	2.5	3.1	2.6
H26d	H27d	2.2	2.6	2.4	H12	Me35	2.3	2.8	2.5
H27d	H27u	1.7	2.1	1.8	H12	Me38	2.8	3.4	3.0
H26d	H26u	1.5	1.9	1.8	H12	Me37	3.5	4.3	3.3
H36d	H36u	1.6	1.9	1.8	H4	H5u	2.1	2.5	2.4
H12	Me35	2.2	2.7	2.6	H4	Me41	2.1	2.5	2.5
H2	Me43	2.3	2.9	2.9	H26d	H27d	2.4	2.9	2.3
H4	Me41	2.3	2.8	2.6	H26d	H26u	1.6	2.0	1.8
H10	Me39	2.3	2.9	2.7	H6	Me40	2.3	2.8	2.6
H12	Me37	2.6	3.2	3.0	H27d	H27u	1.7	2.1	1.8
H10	Me38	2.5	3.1	2.6	H27d	H26u	2.0	2.4	2.4
H12	Me38	2.6	3.1	3.0	H15d	H15u	1.6	1.9	1.7
H15d	H15u	1.6	1.9	1.8	H14	Me35	2.5	3.0	2.6
H6	Me40	2.3	2.8	2.7	H15d	Me35	2.7	3.2	3.0
H14	Me35	2.4	3.0	2.6	H27d	Me32	2.8	3.4	2.5
H15d	Me35	2.7	3.3	3.0	H16	Me34	2.3	2.8	2.5
H8	Me40	2.4	2.9	2.7	H15d	Me34	2.7	3.3	3.0
H8	Me38	2.3	2.8	2.6	H27u	Me32	1.9	2.4	2.5
H6	Me39	2.4	2.9	2.7	H8	Me38	2.3	2.9	2.5
H16	Me34	2.4	2.9	2.6	H8	Me39	2.5	3.1	2.6
H15d	Me34	2.8	3.4	3.0	H18	H15u	2.1	2.6	2.2
H8	Me39	2.6	3.1	2.7	H25	H27u	2.3	2.8	2.4
H22u	Me33	3.0	3.7	3.0					
H23u	Me33	2.9	3.5	4.4					
H10	H8	2.5	3.1	2.9					
H19	Me34	3.8	4.6	3.8					
H20	H22u	2.6	3.2	3.3					
H25	H23u	2.6	3.2	2.8					
H25	H27u	2.4	2.9	2.6					

sterochemistry at each of the stereogenic centres was set to conform with the structure in reference 8 and Fig. 1. For each metal salt the metal ion replaced the acidic hydrogen and the metal to carboxylate covalent bond was broken. The initial conformational set was created by high temperature molecular dynamics and subsequent rapid quenches. Using the starting model 50 ps MD simulation was performed at 1000 K with 1 fs time steps. The resulting conformations were minimised and saved at every 1000 steps. This simulation was run without restraints and was expected to probe the whole of the conformational space available for each of the narasin salts thus providing random initial conformations. In each case the 50 quenched conformations and the starting model form the initial structure set of 51 members.

As in every molecular mechanics or molecular dynamics simulation the results depend critically on the choice of force field. The classical force fields in common use for structure determination from NMR data are designed for and parametrised for proteins, nucleic acids and carbohydrates and so may not be optimal for ionophoric systems with their associated metal ions. Second generation, *e.g.* consistent valence (CVFF) and rule based, *e.g.* extensible systematic (ESFF) force fields

Table 4 Representative metal ion–oxygen distances (pm) in the low energy conformations

Metal–oxygen dist.	Na	K	Rb	Cs
O1	250	288	302	305
O2	262	277	301	298
O3	453	460	518	489
O4	273	284	299	310
O5	254	282	293	299
O6	354	364	344	391
O7	418	429	428	457
O8	396	430	461	397
O9	246	269	292	290
O10	258	280	291	304
O11	374	357	315	335

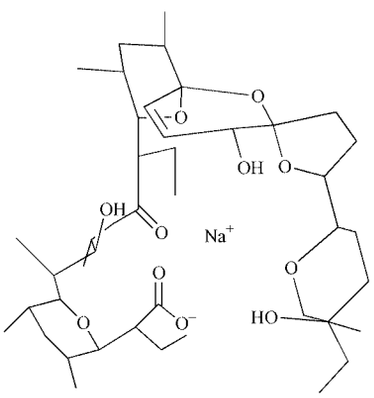

Fig. 1 Final structure for sodium narasin.

cover a wider range of functional groups and so may be appropriate for ionophores. Of these two approaches the ESFF attempts to provide the widest possible coverage of the periodic table with reasonable accuracy. ESFF has been used, for example, to model proteins containing metals. In our previous work on monensin and sodium tetronasin,[16,17] we found that the ESFF force field was much better than the CVFF force field in that the CVFF force field failed to retain the metal ion in the structure even with a relative permittivity of 1 to emphasise the charge–charge interaction. Accordingly we chose to use the ESFF force field for the current study.

For all the salts studied here the simulated annealing (SA) protocol used the random initial conformations, started at 900 K and finished at 10 K. The temperature step was set at 40 K from 900 to 500 K and 10 K from 500 to 10 K. The duration of the steps was 500 fs from 900 to 500 K and 313 fs from 490 to 10 K. A distance-dependent relative permittivity (ε) was initially employed for these SA calculations in which the relative permittivity was scaled proportionately to the charge separation.

The ESFF force field kept the metal ion in the proximity of the oxygen atoms and in each case produced several low energy 'cage-like' conformations with the metal ion in the centre. These low energy structures showed that there is a close contact between both oxygens from the carboxylate group O(2) and O(1) and the metal ion and four other oxygens O(4, 5, 9, and 10). For example in the sodium salt the metal ion is close to (<2.62 Å) O(2), O(1), O(5), O(9) and O(10) and has a relatively close contact with O(4) (2.73 Å) (Table 4).

Comparison of the structures

The general features of the structures are as expected (Figs. 1–4). The oxygen atoms point towards the interior of the molecule providing co-ordination for the metal ion and a hydrophobic exterior surface for the molecule. The six-membered rings are all in chair conformations. Hydrogen bonding involving two or three (sodium salt) of the three hydroxy groups is apparent.

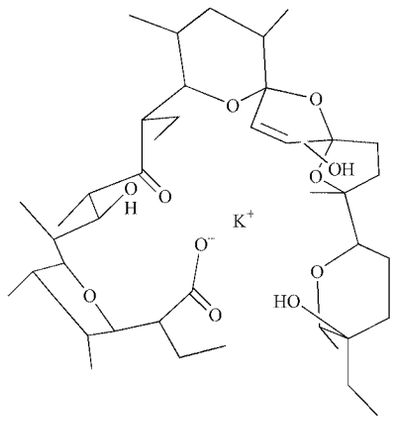

Fig. 2 Final structure for potassium narasin.

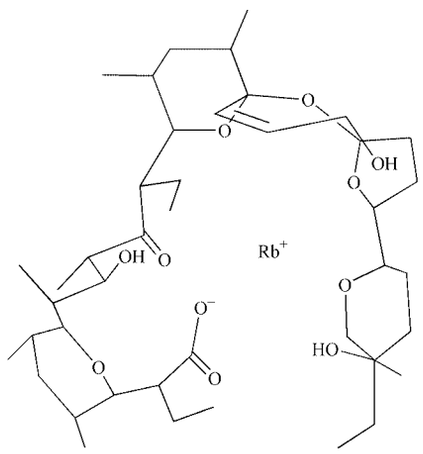

Fig. 3 Final structure for rubidium narasin.

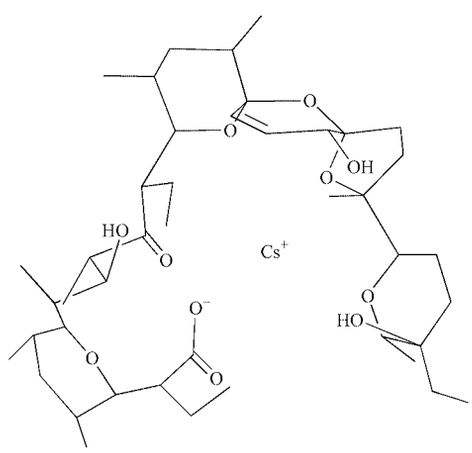

Fig. 4 Final structure for a caesium narasin.

In all the structures the metal ion appears to have strong charge–charge or charge–dipole interactions with six oxygens (Table 4). This is in contrast with earlier results on salinomycin, which only identified up to five co-ordination sites.[14,15] The oxygen to metal distances increase with the larger ionic radius (Table 1). We cannot rule out the presence of a water molecule occupying a seventh bioctahedral co-ordination site.

In all four salts studied the oxygens involved in binding to the metal are O(2), (1), (4), (5), (9) and (10). The narasin molecule seems to be able to retain its co-ordination to the same oxygen atoms as the ionic radius increases in size. This contrasts with monensin where a change in co-ordination pattern is observed as the metal ion size increases from K^+ to Rb^+. The oxygen–metal co-ordination distance does get larger. An approximately stepwise increase can be seen that is of the same size as the increase in the ionic radii seen in Table 1.

Table 5 Average and calculated metal–oxygen distances[a]

	Metal–oxygen distance/pm			
	Na	K	Rb	Cs
Experimental average	257	280	296	301
Calculated distance	242	278	292	307

[a] The calculated distances are based upon a van der Waals radius for oxygen of 140 pm and the ionic radii given in Table 1.

Table 6 Hinge dihedral angles (°) in final structures

		Na	K	Rb	Cs
H2	H3	−158.43	−156.25	−153.3	−164.26
H7	H8	175.16	−179.93	175.99	−178.69
H8	H9	−64.87	−65.18	−65.75	−67.67
H9	H10	179.04	−178.77	−175.89	−178.97
H10	O5	165.6	165.81	160.46	165.05
O5	H12	149.38	149.9	148.61	152.36
H12	H13	67.68	73.57	80.55	77.52
Me33	H25	54.86	59.84	56.77	62.56

In all cases the alkali metal ion is co-ordinated to O(1 and 2) from the carboxylate group. This is similar to our observations on monensin and earlier studies on salinomycin where carboxylate metal ion co-ordination is observed but at variance with the observations of X-ray crystallographers on the closely related sodium monensin.[19,20] This observation reinforces our view, given earlier,[16] that "crystal packing forces" are important in determining the structures of these compounds in the solid state.

To compare the metal–oxygen distances with those expected from published data one can compare the average values for the metal to oxygen distances with the sum of the van der Waals radius of ether oxygen (140 pm) and the ionic radii given in Table 1. These results are presented in Table 5. These values show that the packing of the metal ion is nearly ideal in the potassium and rubidium salts. The packing is somewhat tight in the caesium salt and is comparatively looser in the sodium salt where the experimentally determined average is 15 pm greater than the calculated value. The increase in the relative tightness of the binding as the metal ion size is increased is in accord with larger ions having to fit into a ligand whose size remains constant. The decrease in stability on increasing the metal ion size may well depend in part on this feature.

Comparison of the dihedral angles at the molecular hinges (Table 6) also reveals important changes in the overall conformation of the ligand as the ionic radius varies. It can be seen here that the most important hinge point is between the C(12) and C(13) which, according to our models, increases from 68 to 81° as the metal is changed from sodium through to rubidium but decreases to 78° in the caesium salt. The other hinges are observed to change, but not in a coherent way, with the largest changes occurring about the C(24)–C(25) bond.

It also transpires that the only hinge torsion angle for which a scalar vicinal (^{1}H ^3J) coupling constant change might be measured to confirm the structures is C(12)–C(13). The rising values for this dihedral angle given in Table 6 are those from static models and show the changes to the ligand as the metal ion increases in size. Caughey *et al.*[5] also concluded this is the main hinge point in the molecule but like ourselves could only measure a very small coupling for the Na^+ salt (<0.5 Hz). In our series it also proved difficult to measure this coupling and values observed were *ca.* 1 Hz. Using the modified Karplus equation given in our earlier paper values of around 2.3 Hz are calculated for a 70° dihedral angle. We note that the substitution pattern around the C(12)–C(13) bond in narasin differs from that around the C(20)–C(21) bond in monensin. Variation of the constant employed to correct for substituent electronegativity in the Karplus equation from *ca.* 0.3 used before to *ca.* 0.6 would take the couplings into the observed range.†

Table 7 Hydrogen bonds in narasin salts (distances in pm)

		H-bond OH · · · O distance/pm			
		Na	K	Rb	Cs
OH4	O2	211	217	209	212
OH8	O2	271	393	535	431
OH11	O1	222	220	208	286
OH8	O11	368	335	446	364

Two hydrogen bonds appear in the structures (Table 7). The strongest is between OH(4) and O(2) and is characterised by OH · · · O distances in the 210–220 pm region. The second is from OH(11) to O(1) and is characterised by slightly larger distances. The first of these is present as a strong bond in all of the salts and ties down the structure of the molecules near the acid head group. The second, head to tail, hydrogen bond is present as a strong bond in the Na^+, K^+ and Rb^+ salts but becomes much weaker when the largest ion Cs^+ is present and the relevant OH · · · O distance increases dramatically to 286 pm. There is evidence for a weak hydrogen bond from O(8) to the carboxylate group as proposed by Mronga *et al.* for sodium salinomycin[15] (271 pm) which is not present in the other salts.

Most interestingly the five-membered ring (ring D) changes its conformation in the Rb^+ salt to allow the head to tail (OH(11) to O(1)) hydrogen bond to be retained despite the increase in ion size. It appears that this option is not available to the even larger Cs^+ salt in which ring D reverts to its former conformation and a much weaker head to tail hydrogen bond is seen.

Conclusions

We conclude that narasin accommodates the increasing ionic radius of the alkali metals by several means even though the same set of six oxygens remain co-ordinated to the metal ion. The first is that the metal to oxygen distances increase in line with the increasing atomic radii of the metals. The second is by increases in the HC(12)–HC(13) dihedral angle where changes appear to be easiest. A third is by altering the conformation of the five-membered ring in the Rb^+ salt to permit the head to tail hydrogen bond to be retained. There are two hydrogen bonds present throughout the series between OH(4) and O(2) and between OH(11) and O(1). The largest ion Cs^+ can only be accommodated at the expense of weakening the head to tail hydrogen bond OH(11)–O(1) present in the other salts. There is a weak hydrogen bond between O(8) and O(2) in the sodium salt that is not present in the others. Slight adjustments and conformational changes take place in other parts of the molecule but these changes are barely noticeable.

The results presented in this paper together with our earlier results on the salts of monensin and tetronasin and the X-ray diffraction and NMR studies on salinomycin shed considerable light on the structures of these fascinating molecules. The variability in the patterns of co-ordination to the metal ion, changes in hydrogen bonding, and the backbone flexibility seen here show that these are systems where structures can and do vary readily. This ready variability in ligand conformation and metal ion binding gives the molecules their facile and extremely rapid on/off reactions in the membrane/water interface. These structural studies provide a detailed, qualitative insight into the

† The constant k in the Karplus equation employed in our previous paper[16] was incorrectly stated as 0.74. This is in fact the value of $1 - k$. The constant k should, therefore, have been given as 0.26.

mechanisms of the ion association and the membrane transport processes.

Experimental

NMR Sample preparation of narasin salts

Narasin acid salt (10 mg) obtained from Eli Lilly & Co. (reference sample) was dissolved in 1 cm^3 of $CDCl_3$. To this a saturated aqueous sodium/potassium/rubidium/caesium carbonate solution (*ca*. 2 cm^3) was added and the mixture was stirred vigorously for 1 hour. After stirring the mixture was allowed to settle for approximately 15 minutes. The chloroform layer was separated and filtered through a small amount of the anhydrous metal carbonate. All of the NMR samples were degassed by bubbling oxygen free nitrogen gas through the sample.

NMR Measurements

All the spectra were obtained on a Varian Unity 500+ spectrometer at 298 K using the solvent peak at 7.27 ppm as indirect reference to TMS at 0 ppm. The proton chemical shifts were checked against the published data with the help of COSY and NOESY spectra. The 2D experiments were run with 1024 complex data points in *t*1 and 512 complex data points in the *t*2 domain and 16 transients were acquired for each increment. For processing a cosine bell function was applied before transformation except for the COSY spectra for which a sine bell function was used. All spectra were zero filled once in both dimensions. The mixing time was 400 ms for NOESY experiments, which gave the best signal to noise ratio in the linear region of the NOE build up curves. The distances from the NOESY cross-peak intensities were calculated by application of the isolated spin pair approximation using an approximate average of a geminal proton–proton distance of 1.78 Å as reference.

Molecular mechanics

All molecular mechanics simulations were carried out on Silicon Graphics O2 and INDY computers using MSI/Biosym's CDiscover (Discover 97) software package in Insight II environment. The simulation protocols were written in Biosym's BTCL language. For the energy calculation the extensible systematic force field (ESFF) was used with 9.5 Å cut-off for van der Waals and Coulomb interactions. During the molecular dynamics calculations the velocity Verlet integrator and 1 femtosecond timestep were used. The temperature was controlled by direct velocity scaling with a 10 K temperature window. The relative permittivity was distance dependent with the upper limit of 4.5 to take into account the solvent effect at this level.

The starting model was built by using the 'builder' program from Insight II and the stereocentre conformations were altered according to a previous published structure. The initial conformation set was created by high temperature molecular dynamics and subsequent rapid quenches. Using the starting model 50 ps MD simulations were performed at 1000 K with a 1 fs time step, and the resulting conformations were minimised and saved after every 1000 steps. The simulation was run without restraints, so the procedure was expected to discover the whole conformation space and to provide random initial conformation states.

Restrained simulated annealing was run with 54 restraints for the sodium narasin salt, 53 for the potassium narasin salt, 57 for the rubidium narasin salt and 52 for the caesium narasin salt. The SA protocol was carried out with 900 K as the initial and 10 K as the final temperature. The temperature step was set at 40 K from 900 to 500 K and 7.5 K from 490 to 10 K. The duration was 500 fs from 900 to 500 K and 313 fs from 490 to 10 K at every step. Minimisation was applied after every simulated annealing in cascade manner: steepest-descent, conjugate gradient (Fletcher algorithm), Newton method (BFGS algorithm). The iteration limit was 1500 steps, and the final convergence criterion was 0.001 as maximum derivative.

In order to reveal the dynamic behaviour of our minimised static model 100 ps restrained molecular dynamics was run at 298 K. The trajectory was updated in every 0.1 ps.

The consistency of the most likely conformer with the experimental data was checked by the back-calculation of the experimental data based on the trajectory of 100 ps restrained molecular dynamics simulation. The back-calculation was performed using the program 'MDNOE,' written by S. Homans, which implements the RMA approach. During the back-calculation the fast internal motion model has been applied, which holds for ionophores in non-polar solvents. The correlation time was estimated to 0.2 ns by the comparison of the diagonal peak and the off-diagonal peak for both the calculated and back-calculated values of their intensities.

Acknowledgements

We thank the British Council and OMFB (Budapest) for a combined grant, which facilitated this work.

References

1 F. G. Riddell, *Chem. Br.*, 1992, 533.
2 G. R. Painter and B. C. Pressman, *Biochem. Biophys. Res. Commun.*, 1979, **91**, 1117.
3 H. Seto, T. Yahagi, Y. Miyazaki and N. Otake, *J. Antibiot.*, 1977, **30**, 530.
4 D. H. Berg and R. L. Hamill, *J. Antibiot.*, 1978, **31**, 1.
5 B. Caughey, G. R. Painter, B. C. Pressman and W. A. Gibbons, *Biochem. Biophys. Res. Commun.*, 1983, **113**, 832.
6 F. G. Riddell and S. J. Tompsett, *Tetrahedron*, 1991, **47**, 10109.
7 M. J. O. Antenius and N. A. Rodios, *Bull. Soc. Chim. Belg.*, 1981, **90**, 715.
8 D. Haynes and H. Staerk, *J. Membrane Biol.*, 1974, **17**, 313.
9 D. Haynes, *J. Membrane Biol.*, 1974, **17**, 341.
10 F. G. Riddell and S. J. Tompsett, *Biochim. Biophys. Acta*, 1990, **1024**, 193.
11 B. C. Pressman and G. R. Painter, "The Mechanism of the Biological Effects of Carboxylic Ionophores: Modulation of Intracellular Activity by Na^+", in *The Biochemistry of Biological Processes*, ed. F. W. Strattman, Elsevier, Amsterdam, pp. 41–54.
12 G. R. Painter and B. C. Pressman, *Top. Curr. Chem.*, 1982, **101**, 83.
13 B. Caughey, G. R. Painter and W. A. Gibbons, *Biochem. Pharmacol.*, 1986, **35**, 4103.
14 E. Paulus, M. Kurz, H. Matter and L Vertesy, *J. Am. Chem. Soc.*, 1998, **120**, 8209.
15 S. Mronga, G. Muller, J. Fischer and F. G. Riddell, *J. Am. Chem. Soc.*, 1993, **115**, 841.
16 T. Martinek, F. G. Riddell, C. Wilson and C. T. Weller, *J. Chem. Soc., Perkin Trans. 2*, 2000, 34.
17 T. Martinek, F. G. Riddell, T. J Rutherford, S. Sareth and C. T. Weller, *J. Chem. Soc., Chem. Commun.*, 1998, 1893.
18 D. T. Richens, *The Chemistry of the Aqua Ions*, Wiley, Chichester, 1997.
19 W. L. Duax, G. D. Smith and P. D. Strong, *J. Am. Chem. Soc.*, 1980, **102**, 6725.
20 P. Y. Barrans, M. Alleume and G. Jeminet, *Acta Crystallogr., Sect. B*, 1982, **38**, 1144.